Physica D 46 (1990) 254–264
North-Holland

RELATIONSHIP BETWEEN THE FRACTAL DIMENSION AND THE POWER LAW INDEX FOR A TIME SERIES: A NUMERICAL INVESTIGATION

T. HIGUCHI
The Institute of Statistical Mathematics, 4-6-7 Minami-Azabu, Minato-ku, Tokyo 106, Japan

Received 29 June 1989
Revised manuscript received 4 February 1990
Accepted 15 March 1990
Communicated by M. Mimura

A time series showing self-affine over all time scales follows a power law spectrum; when such a time series, $X(j)$ ($j = 1, 2, \ldots, N$), is transformed into the discrete Fourier transformation (i.e. $X(j) = \sum_{k=0}^{N/2} C_k \cos(2\pi jk/N - \theta_k)$, where C_k and θ_k are the amplitude and phase for wavenumber k, respectively), the power spectrum density for wavenumber k is given by $P(k) = C_k^2/N \propto k^{-\alpha}$. The relationship between the power law index α and the fractal dimension D for a time series following a power law spectrum is investigated by using a numerical experiment. It should be noted that the time series with the same power law index shows various behaviors in a time domain, depending on distribution of θ_k, and gives different values of the fractal dimension accordingly. In short, the phase distribution strongly affects the irregularity represented in terms of the fractal dimension. In addition, the relationships between α and D are also examined both for the differenced and for the integrated time series.

1. Introduction

The power spectrum analysis is generally used for examining an irregular time series. When a power spectrum density $P(f)$ shows, in particular, a red-noise type without an eminent peak, it is naturally approximated to follow a power law spectrum: $P(f) \propto f^{-\alpha}$, where the red-noise type indicates that the power spectrum exhibits appreciably more power at low frequencies than at high frequencies, i.e. $\alpha > 0$. This approximation to the power spectrum is the simplest description for the red-noise type. In this approximation, the power law index α is one of the quantities describing the irregularity of the time series. Such recipe is often applied to time series observed in many fields.

A new concept for describing the characteristics of irregular time series has been presented by Mandelbrot [1]. He considered the fractal set of points $(t, X(t))$ forming the graph of a function X defined on the unit interval [1, 2]. In short, when the time series $X(t)$ can be viewed geometrically as a curve, he defined a statistically self-affine curve of which each part can be considered as a reduced scale image of the whole. By setting $X(0) = 0$, the rescaled function $t^{-H}X(t)$ has a probability distribution independent of t, where H is an index describing the characteristics of the self-affine curve. H can be allowed to lie anywhere in the range of $0 < H < 1$. Mandelbrot called this curve the *Brown* line-to-line function. (We call hereafter this function BLF for short.) In terms of a spectrum analysis, the power spectrum density of such curve follows a power law form, $P(f) \propto f^{-1-2H}$ [1, 3].

In order to obtain the fractal dimension D of the time series, Burlaga and Klein presented a method to calculate the length of the curve of the time series [4]. They compared the power law index α obtained directly from the FFT procedure with that estimated from the fractal dimen-

sion using the fractional relationship between α and D: $\alpha = 5 - 2D$ [1, 3]. Their emphasis is laid on the efficiency of the fractal analysis as compared with that of the power spectrum analysis.

Another method to calculate the curve length of the time series has been proposed by Higuchi [5]. As for the accurate estimation of the fractal dimension, the superiority of his method to that by Burlaga and Klein was demonstrated. He has also shown that his method is superior to the power spectral analysis in the stable estimation of the index, particularly when the number of the data used for estimating the indices is limited. Such case often occurs in the analysis of geophysical phenomena. For example, the weak stationarity can be assumed only during a short time interval, and the number of the data used in the estimation of the indices comes to be limited accordingly. The fractal analysis has been used for the description of the irregularity of the set of points $(t, X(t))$, not only for the time series [4–6] but also for the topographic profile [7, 8].

The relationship between the fractal dimension and the power law index is unsettled for a general time series showing the power law spectrum. Our major object is to investigate the relationship between them by using a numerical experiment.

2. Relationship between the fractal dimension and the power law index

First, we give an outline of the method presented by Higuchi [5]. From a given time series $X(j)$ $(j = 1, 2, 3, \ldots, N)$, we first construct a new time series, X_τ^m, defined as follows:

$$X_\tau^m; X(m), X(m+\tau), X(m+2\tau), \ldots, X(m+[(N-m)/\tau]\tau) \quad (m = 1, 2, \ldots, \tau), \tag{1}$$

where [ ] denotes the Gauss' notation and both τ and m are integer. The length of the curve, X_τ^m, is given by

$$L_m(\tau) = \left\{ \left(\sum_{i=1}^{[(N-m)/\tau]} |X(m+i\tau) - X(m+(i-1)\tau)| \right) \times \frac{N-1}{[(N-m)/\tau]\tau} \right\} \frac{1}{\tau}. \tag{2}$$

We define the curve length for the time interval of τ as the average value over τ sets of $L_m(\tau)$, and specify it by $\langle L(\tau) \rangle$. If $\langle L(\tau) \rangle \propto \tau^{-D}$ within the range $\tau_{\min} \le \tau \le \tau_{\max}$, the curve is self-affine with fractal dimension D in this range.

The time series showing self-affine over all time scales has a power law spectrum: $P(f) \propto f^{-\alpha}$, where $P(f)$ is the power spectrum density. For BLF, the power law index α is related to the fractal dimension D of the graph of $X(j)$ by

$$\alpha = 5 - 2D \tag{3}$$

for $1 < D < 2$ [1, 3]. Nevertheless, the relationship between the fractal dimension and the power law index is unsettled for a general time series showing the power law spectrum. We therefore investigate it by using a numerical experiment.

When the total data number N is even, $X(j)$ can be expressed in terms of the discrete Fourier transformation as follows:

$$X(j) = \sum_{k=0}^{N/2} A_k \cos(2\pi jk/N) + \sum_{k=1}^{N/2-1} B_k \sin(2\pi jk/N) = \sum_{k=0}^{N/2} C_k \cos(2\pi jk/N - \theta_k), \tag{4}$$

where $C_k = \sqrt{A_k^2 + B_k^2}$ and $\theta_k = \tan^{-1}(B_k/A_k)$ $(k \neq 0, N/2)$. For $k = 0$ and $k = N/2$, C_k is given by A_k. $\theta_{N/2}$ and θ_0 should be zero due to the degree of freedom. C_k and θ_k represent the amplitude and phase for wavenumber k, respec-

tively. We remark here that whether N is even or odd, does not affect the following results investigated in this study. The power spectrum density for wavenumber k is given by

$$P(k) = C_k^2/N. \tag{5}$$

Obviously, a power spectrum has no information about the phase; the variable θ_k disappears in eq.(5).

We consider the time series following the power law spectrum

$$P(k) = Qk^{-\alpha}, \tag{6}$$

where α is a power law index and Q is a certain constant. When values of α and Q are given, the amplitude for wavenumber k, C_k can be defined by using eqs. (5) and (6), except for C_0. No value of C_0 can satisfy the power law spectrum in eq. (6). Nevertheless, the graph $(j, X(j))$ is shifted only in vertical direction, according to C_0, and thereby the behavior of the graph is independent of C_0. In other words, C_0 is a threshold value interrelated with the mean of $X(j)$, and hence we set $C_0 = 0$ in this study.

Next, we must determine the phase for wavenumber k, θ_k, in order to construct simulated data following a power law spectrum. For simplicity, θ_k is given by a random variable with a uniform distribution of the range $[0, \theta_{\max}]$ ($\theta_k \sim U([0, \theta_{\max}])$), where $\theta_{\max}$ is given in degree. $\theta_{\max}$ can vary within a range of [0,360]. The correlation between the phases is set to be $\langle \theta_k \cdot \theta_{k'} \rangle = \delta_{kk'}$, where δ_{ij} denotes the *Kronecker* delta.

We show in figs. 1a–1e the time series with $\theta_{\max} = 0$, 30, 60, 120, and 360 for the power law index $\alpha = 2$. When $\alpha = 2$, $\theta_{\max} = 360$ gives a time series showing a one-dimensional *Brownian* motion along the vertical axis. It is seen that the time series shows irregular behavior with an increasing value of $\theta_{\max}$. It is generally thought on a visual inspection of panels (a)–(e) that the disturbance in the high-frequency domain becomes enhanced as increasing in $\theta_{\max}$. In fact, the time series shown in panels (a)–(e) possess the same power spectrum. By comparing the variation shown in panel (a) with that in panel (e), it is clear that the distribution of θ_k strongly affects behavior in the time domain. Then, a quantitative analysis using only a power law index is inappropriate for describing the irregularity of the time series. It is necessary to take the information of the phase distribution into the quantitative analysis of the time series.

We examine the dependency of the probability distribution of θ_k on the fractal dimension D as a function of $\theta_{\max}$. The values of the fractal dimension D are shown in fig. 2a as a function of $\theta_{\max}$ for several values of the power law index: $\alpha = 1$, $3/2$, 2, $5/2$, and 3. The total data number used in this calculation is $N = 2^{17}$ ($\tau_{\min} = 1$ and $\tau_{\max} = 2^{11}$). It is clear from fig. 2a that the fractal dimension strongly depends on the probability distribution of the phase. Since the probability distribution of θ_k, $P(\theta_k)$, is a uniform distribution given by $1/\theta_{\max}$, the variable $\log(\theta_{\max})$ is proportional to the quantity $E(\theta_{\max})$, which is defined by

$$\begin{aligned} E(\theta_{\max}) &= -\sum_{k=1}^{N/2-1} \int_0^{\theta_{\max}} P(\theta_k) \log P(\theta_k)\, \mathrm{d}\theta_k \\ &= (N/2 - 1) \log(\theta_{\max}). \end{aligned} \tag{7}$$

This quantity, $E(\theta_{\max})$, represents the randomness of the probability distribution of the phase, which is naturally based on the entropy of the probability distribution [9, 10]. Hence we call this variable, $E(\theta_{\max})$, *phase entropy*. To examine the dependency of D on E, we show in fig. 2b the values of D against $\log(\theta_{\max})$. We can see in fig. 2b that the value of the fractal dimension linearly increases as E increases within the range $\theta_{\max} \leq 180$ for every power law index. The special value $\theta_{\max} = 0$ is of particular interest. In this study, the numerical experiments show a tendency that the fractal dimension converges to $D = 1$, at least for $2 \leq \alpha$. For the range of $180 \leq \theta_{\max}$, the whole curve flattens and the fractal dimension reaches

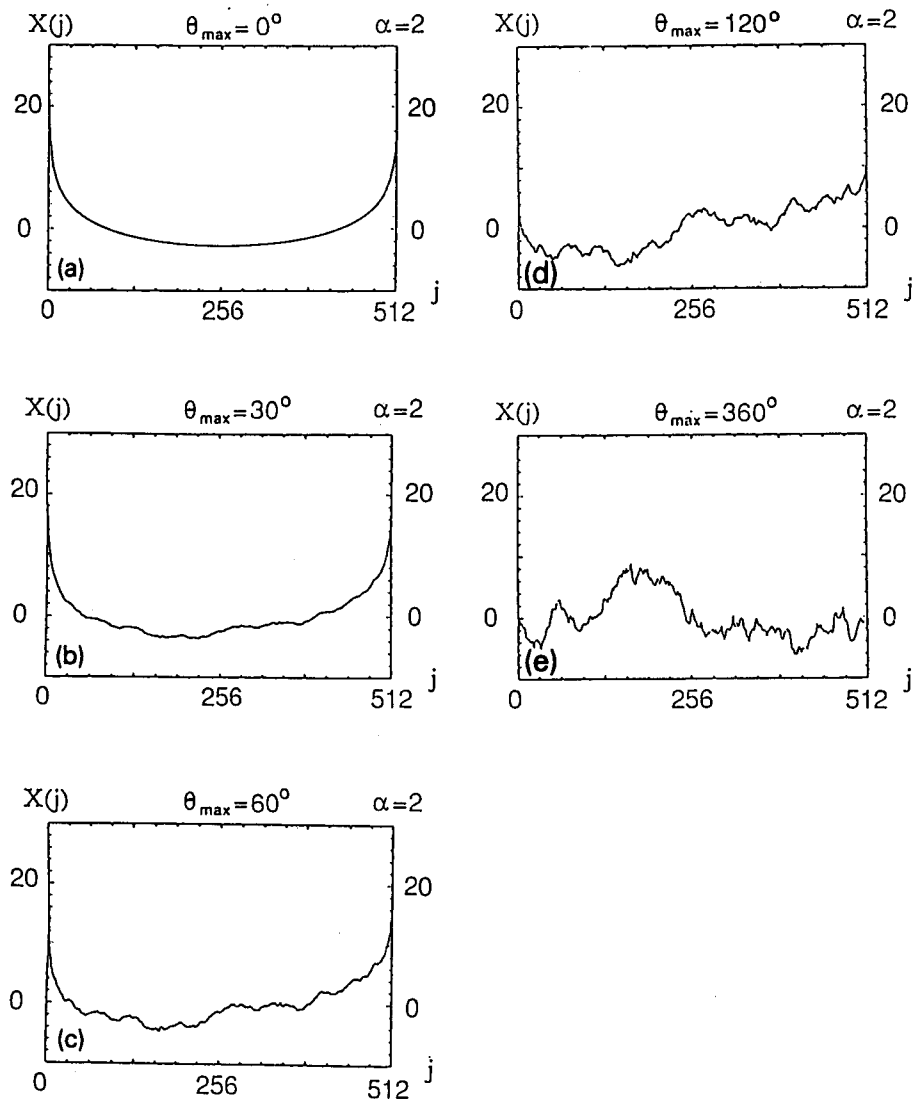

Fig. 1. The simulated time series with power law index $\alpha = 2$ for several values of θ_{max}, where θ_{max} is a parameter describing the distribution of the phase of the wave number k. Panels (a)–(e) correspond to the time series with $\theta_{max} = 0$, 30, 60, 120, and 360, respectively.

the value independent of θ_{max}, according to the power law index α.

The power spectrum of BLF follows a single power law ($P(f) \propto f^{-\alpha}$) over the whole frequency range and the fractal dimension is interrelated to the power law index by eq. (3). In addition, it should be noticed that the BLF curve has a probability distribution of the phase with $\theta_{max} = 360$. Since the range $1 < D < 2$ in eq. (3) implies that the power law index α can be allowed to lie within the range $1 < \alpha < 3$, it is interesting to examine the fractal dimension D of a red-noise type time series within the ranges $0 \leq \alpha \leq 1$ and $3 \leq \alpha$.

We examine the relation of eq. (3) for the range $0 \leq \alpha \leq 4$ by calculating the fractal dimension of the simulated time series which follows a single power law spectrum. Of course, θ_{max} should be 360 for all time series. Fig. 3 shows the fractal dimension D against the power law index α. A straight line indicates the relationship of eq. (3). The curve is in good accordance with a straight line near $\alpha = 2$. When increasing α from 2 to 3, D becomes slightly greater than that given by eq.

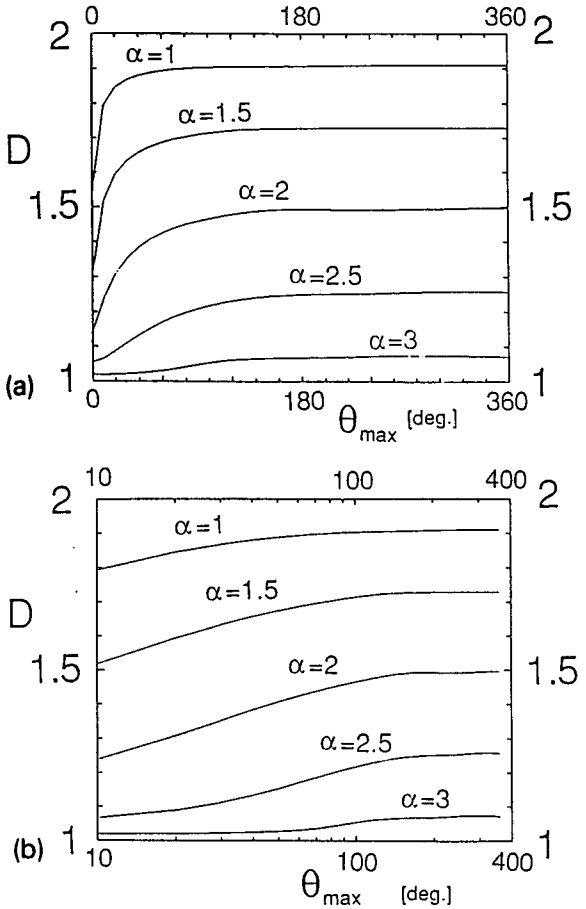

Fig. 2. The fractal dimension D as a function of θ_{max} (a) and of $\log(\theta_{max})$ (b) for several power law indices: $\alpha = 1$, 3/2, 2, 5/2, and 3.

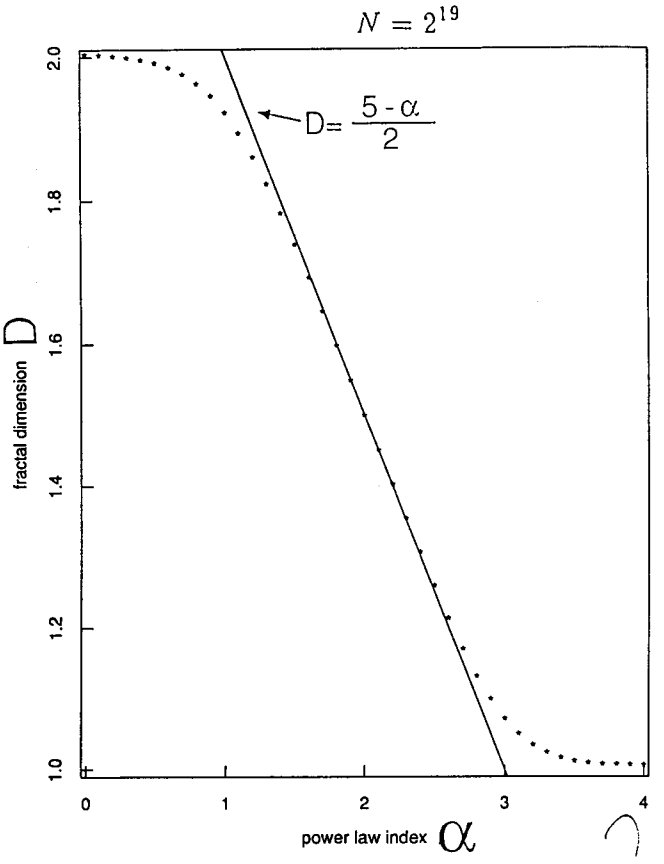

Fig. 3. The calculated fractal dimension D as a function of the power law index α. In this calculation, we set $N = 2^{19}$, $\tau_{min} = 2^4$, and $\tau_{max} = 2^{13}$. The straight line indicates the relationship of eq. (3).

(3). On the contrary, D becomes smaller than that given by eq. (3) for α of less than 2. Then, the relationship defined by eq. (3) completely holds in the vicinity of $\alpha = 2$ (3/2–5/2).

Fox [8] also examined the relationship of the fractal dimension with the spectral exponent (corresponding to the power law index α in this study) for the BLF curve. To calculate the fractal dimension, he used the divider method, which gives an erroneous fractal dimension depending on the scale of $X(j)$ [11]. The present result is closer to the relationship of eq. (3) and looks more symmetric than his result.

We examine the dependency of D on the total data number N in order to investigate the discrepancy of D from the value given by eq. (3) around $\alpha = 1$ and $\alpha = 3$. Time series with data number N ($N = 2^m$, $m = 14, \ldots, 19$) are generated according to the aforementioned procedure. The values of D for these simulated time series are calculated as a function of α, and the results for $N = 2^{15}$, 2^{17}, and 2^{19} are shown in fig. 4. The three curves coincide around $\alpha = 2$ (3/2–5/2), representing good agreement with eq. (3). For any curve, the deviation from the straight line given by eq. (3) shows a tendency similar to that seen in fig. 3. However, for any α, the residual from the straight line becomes smaller when increasing N. In short, the curve approaches a straight line (indicated by arrows) for the range $1 < \alpha < 3$, and flattens with $D = 2$ for $0 < \alpha < 1$ and with $D = 1$ for $3 < \alpha < 4$.

To clearly demonstrate this tendency, the values of D are shown in figs. 5a and 5b against $\log_2 N$ for $\alpha = 1$ and $\alpha = 3$, respectively. As mentioned above, we can see in these figures that $D \to 2$ (a) and $D \to 1$ (b) when increasing N.

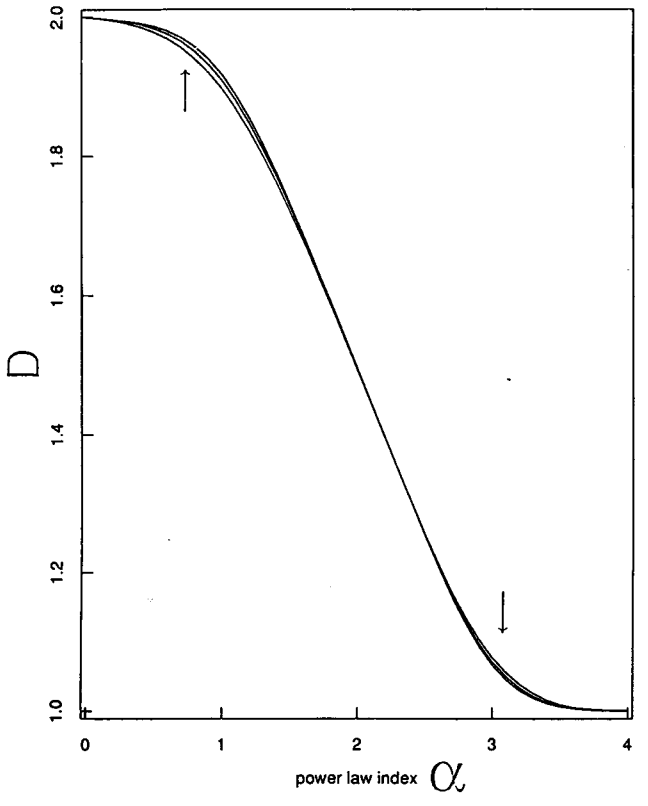

Fig. 4. D as a function of α for $N = 2^{15}$, $N = 2^{17}$, and $N = 2^{19}$. ($\tau_{min} = 2^4$ and $\tau_{max} = 2^{13}$.)

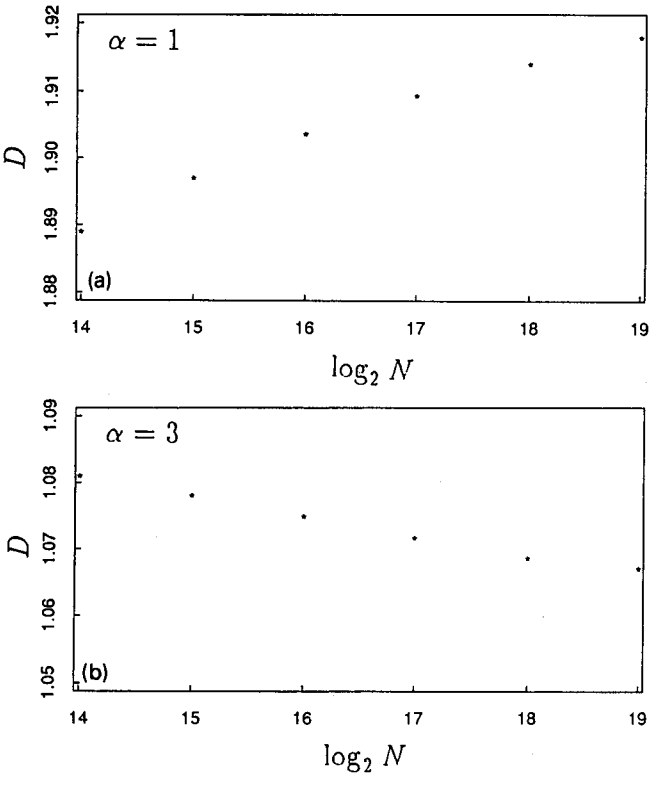

Fig. 5. The fractal dimension D plotted against the logarithm of the data number, $\log_2 N$, for $\alpha = 1$ (a) and $\alpha = 3$ (b).

Nevertheless, we cannot confirm a convergence of $D = 1$ or $D = 2$ as $N \to \infty$ because of the computational limitation, such as memory.

3. The fractal dimensions of the differenced and integrated time series

We consider the problem of estimating α when D is given. Since D corresponds to α one-to-one within $1 < \alpha < 3$, α can be estimated through eq. (3) if $1 < D < 2$. Nevertheless we cannot get the value of α for the cases of $D = 1$ and $D = 2$, because, as demonstrated in figs. 3 and 4, the ranges $0 < \alpha < 1$ and $3 < \alpha$ correspond to $D = 2$ and $D = 1$, respectively, Moreover, the values of D around $\alpha = 1$ and $\alpha = 3$ partly dependent on N. Consequently, we should not estimate the value of α for $D \simeq 1$ or $D \simeq 2$.

To resolve the degenerations of α: $[0, 1] \to D$: 2 and α: $[3, \infty) \to D$: 1, we consider the differenced and integrated series of the original time series. The differenced time series is given by

$$\nabla X(j) = X(j+1) - X(j) \quad (j = 1, \ldots, N-1), \tag{8}$$

and the integrated one is given by

$$X_\Sigma(j) = \sum_{l=1}^{j} X(l) \quad (j = 1, \ldots, N). \tag{9}$$

$\nabla X(j)$ is the forward first-order difference of $X(j)$ and $X_\Sigma(j)$ is an increment process of $X(j)$. We designate the fractal dimensions of $\nabla X(j)$ and $X_\Sigma(j)$ by D_∇ and D_Σ, respectively. Similarly, the power law indices for $\nabla X(j)$ and $X_\Sigma(j)$ are denoted by α_∇ and α_Σ, respectively.

The difference operator ∇ for the time series represented by eq. (4) is possibly replaced by a multiplication of k. Then, when the power spectrum density is given by eq. (6), the power spec-

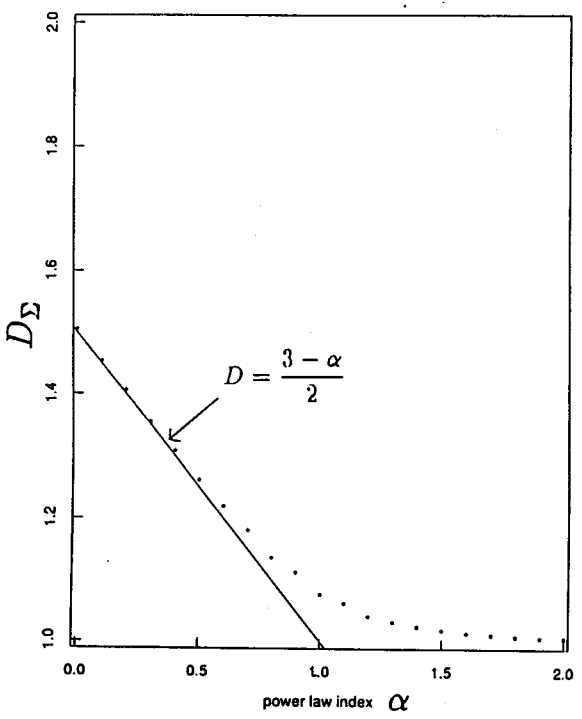

Fig. 6. The fractal dimension of the integrated time series, D_Σ, as a function of α. In this calculation, we use $N = 2^{19}$, $\tau_{min} = 2^4$, and $\tau_{max} = 2^{13}$. The straight line is given by $D = (3-\alpha)/2$.

trum density of the differenced time series shows $P(k) \propto k^{-\alpha+2}$. It is easily understood from eqs. (8) and (9) that $\alpha_\nabla = \alpha - 2$ and $\alpha_\Sigma = \alpha + 2$. Thus far, we get the following correspondence: α: $(3,5) \rightarrow \alpha_\nabla$: $(1,3)$ and α: $(0,1) \rightarrow \alpha_\Sigma$: $(2,3)$. Since α within $1 < \alpha < 3$ maps D one-to-one (approximately given by eq. (3)), we conjecture that the mappings f: $\alpha \rightarrow D_\nabla$ and f: $\alpha \rightarrow D_\Sigma$ are likely given by the curve demonstrated in fig. 3 (f: $\alpha \rightarrow D$).

We show in fig. 6 D_Σ as a function of α. The straight line drawn in fig. 6 is defined by $D = (3-\alpha)/2$. As previously estimated, the curve of f: $\alpha \rightarrow D_\Sigma$ shows a curve highly similar to the one shown in fig. 3. If the curve in fig. 3 is shifted by -2 along the α axis, it is identical with the curve shown in fig. 6. D_∇ is plotted in fig. 7 against α. The straight line indicates $D = (7-\alpha)/2$. By shifting horizontally the original curve (shown in fig. 3) by 2, this curve exactly agrees with that in fig. 7. In both cases of f: $\alpha \rightarrow D_\Sigma$ and f: $\alpha \rightarrow D_\nabla$, the discrepancy from the straight line, which is

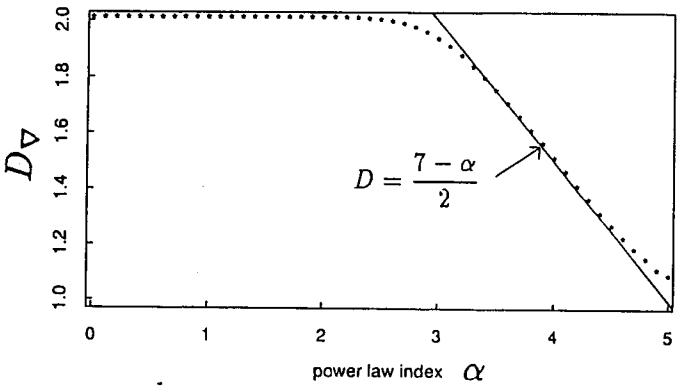

Fig. 7. The fractal dimension of the differenced time series ($N = 2^{19} - 1$), D_∇, as a function of α. For any α, $\tau_{min} = 2^4$ and $\tau_{max} = 2^{13}$. The straight line indicates $D = (7-\alpha)/2$.

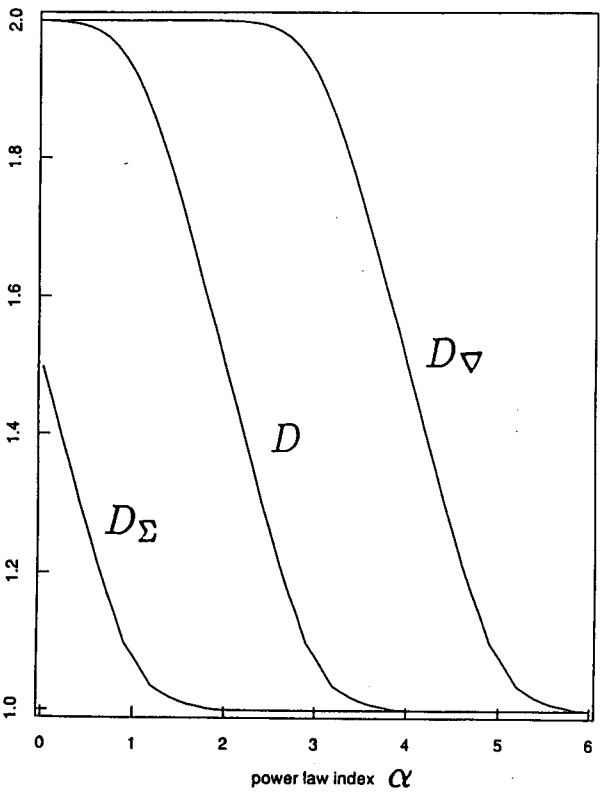

Fig. 8. D, D_Σ, and D_∇ are schematically shown as a function of the power law index α.

seen in fig. 3 around $\alpha = 1$ and $\alpha = 3$, is also pointed out.

We schematically summarize these results in fig. 8. Although any time series with α $(0 < \alpha < 1)$ has $D = 2$, D_Σ corresponds to α one-to-one. The relationship is approximately given by $D_\Sigma = (3-\alpha)/2$. Similarly, the degeneration of $D = 1$ for $3 < \alpha < 5$ can be satisfactorily resolved by

calculating D_∇. In this case, the mapping is $D_\nabla = (7-\alpha)/2$. In short, a mth-order difference operation to $X(j)$ leads to a horizontal shift by $2m$ of the original curve of D. According to these results, we can get the following relationship:

$$D_{\nabla^m} = (2m + 5 - \alpha)/2 \times (m = -1, 0, 1, \ldots), \quad (10)$$

where ∇^m is an mth order difference operation, but ∇^{-1} means integration. This relationship holds within the α domain of definition $(2m+1, 2m+3)$. However, for $m = -1$, the range is limited to [0, 1).

According to eq. (10), we can estimate α of $X(j)$ by calculating D, D_Σ, and D_∇. In particular, we should compute D_Σ (D_∇) for $D \simeq 2$ (for $D \simeq 1$). However, even if we get the values of D and D_Σ, the value of $\alpha = 1$ ($1/f$ *noise*) cannot be precisely estimated because both D and D_Σ deviate from the straight lines, depending on N. As for $\alpha = 3$, neither D nor D_∇ gives a correct value of α.

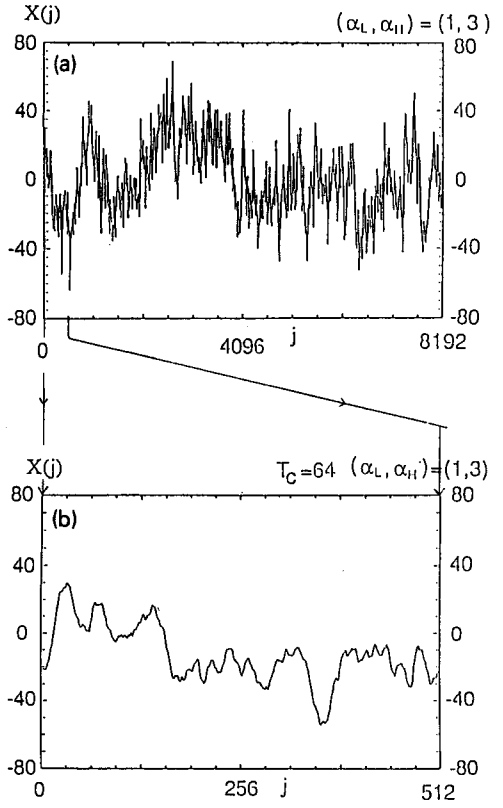

Fig. 9. The simulated time series with power law indices $(\alpha_L, \alpha_H) = (1, 3)$ and the random phase are shown, where α_H and α_L are power law indices defined in the whole frequency range above and below the characteristic frequency f_c, respectively.

4. Time series having a characteristic frequency

When a power spectrum density of a time series $P(f)$ varies as $f^{-\alpha}$ throughout the whole frequency range, the relation between the power law index and fractal dimension was well understood in the previous sections. Next, we consider a time series whose power spectrum density can be described as follows: $P(f) \propto f^{-\alpha_L}$ and $P(f) \propto f^{-\alpha_H}$ in a low- and a high-frequency domain, respectively. The frequency at which the power law index changes is hereafter designated as f_c. In a discrete Fourier expansion of eq. (4), f_c is given by k_c/N, where k_c is the wavenumber where the power law index α in eq. (6) changes. The characteristic period T_c, defined by $1/f_c$, is $T_c = N/k_c$ accordingly. At k_c, we set $Q_L k_c^{-\alpha_L} = Q_H k_c^{-\alpha_H}$, where Q_L and Q_H are constant values. For such time series, whose power spectrum density changes its power law index at k_c, the relationship between the fractal and power spectrum analyses has not yet been examined.

We show in fig. 9 the numerically generated time series with $(\alpha_L, \alpha_H) = (1, 3)$ and random phase. Of course, the random phase means a probability distribution of the phase with $\theta_{max} = 360$. The fractal analysis is applied to such time series ($N = 2^{16}$) and the $\log \tau$ versus $\log\langle L(\tau)\rangle$ plots are demonstrated in fig. 10a. The values of $\log\langle L(\tau)\rangle$ shown in this figure are obtained by averaging over the values of $\log\langle L(\tau)\rangle$ of 500 time series with $(\alpha_L, \alpha_H) = (1, 3)$ and the random phase. When a curve is self-affine for all τ from 1 to τ_{max}, the $\log \tau$ versus $\log\langle L(\tau)\rangle$ plots fall on a straight line for all τ. However, when the $\log \tau$ versus $\log\langle L(\tau)\rangle$ plots show a straight line with a sharp bent at a certain τ, the behavior having a time scale longer than this characteristic time

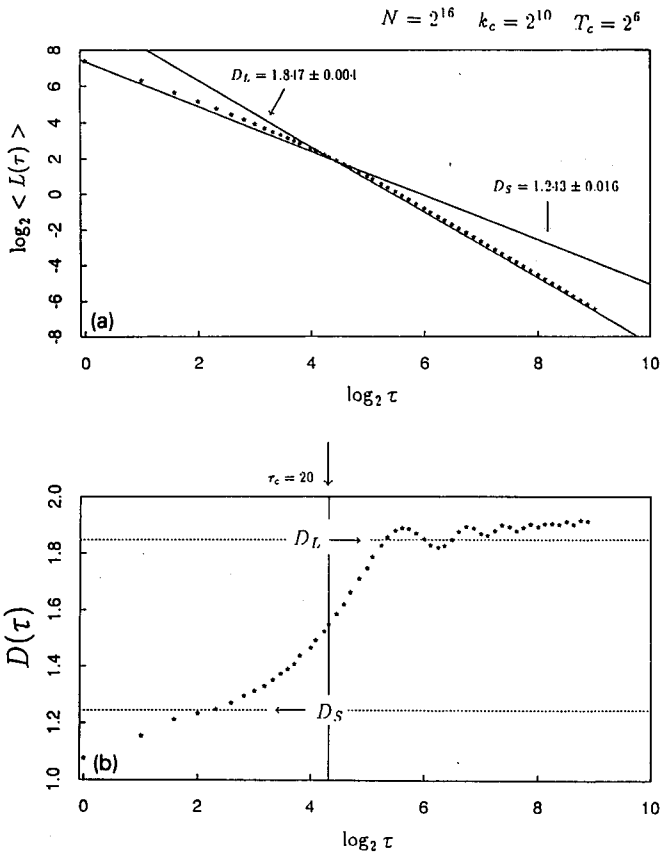

Fig. 10. (a) $\langle L(\tau)\rangle$ of the times series with $(\alpha_L, \alpha_H) = (1, 3)$ and $N = 2^{16}$ as a function of the lag time τ on doubly logarithmic scale. The phase distribution is random. The characteristic wavenumber k_c is set to be 2^{10}, then T_c is 2^6 ($f_c = 2^{10}/2^{16}$). Straight lines with a slope equal to -1.847 and -1.243 are drawn in the time scale longer and smaller than $\tau = 20$, respectively. (b) $D(\tau)$ is plotted against $\log_2\tau$.

scale is different from that shorter than it. We designate this characteristic (critical) time scale by τ_c. Since self-affinity holds within each time scale shorter and longer than τ_c, two fractal dimensions can be defined for such time series. The fractal dimensions defined within the time scales below and above τ_c are specified here by D_S and D_L, respectively. In order to obtain D_S, D_L, and τ_c, a curve consisting of two line segments with a discontinuity in its slope is fitted to the $\log\tau$ versus $\log\langle L(\tau)\rangle$ plots. We call hereinafter this curve the two-segment curve. The two-segment curve is fitted to the $\log\tau$ versus $\log\langle L(\tau)\rangle$ plots by using a least-squares estimation. The characteristic time scale τ_c corresponds to the broken point where the line discontinuously changes its slope. It is seen in fig. 10a that the curve breaks at $\tau_c = 20$. τ_c normalized by the characteristic period T_c, τ_c/T_c, is $20/64$. The two straight lines are also drawn in this figure by vertically shifting so as not to stain the $\log\tau$ versus $\log\langle L(\tau)\rangle$ plots.

Although it maybe appears that the two-segment curve drawn in fig. 10a is satisfactorily fitted to the $\log\tau$ versus $\log\langle L(\tau)\rangle$ plots, the $\log\tau$ versus $\log\langle L(\tau)\rangle$ plots show a round corner around τ_c. Since the fractal dimension D is defined by minus the slope of the straight line fitted to the $\log\tau$ versus $\log\langle L(\tau)\rangle$ plots, it can be considered that minus the differential coefficient of the curve of the $\log\tau$ versus $\log\langle L(\tau)\rangle$ plots is replaced by D. We extend the definition of D as follows:

$$D(\tau) \equiv -\frac{\mathrm{d}\log\langle L(\tau)\rangle}{\mathrm{d}\log\tau} \simeq -\frac{\nabla\log\langle L(\tau)\rangle}{\nabla\log\tau}. \tag{11}$$

We show in fig. 10b $D(\tau)$ as a function of $\log_2\tau$. The two dotted horizontal lines superposed in this figure indicate the values of D_L and D_S, which are obtained by fitting the two-segment curve shown in fig. 10a. $D(\tau)$ gradually becomes larger as τ increases, and then saturates at $D \simeq 1.9$ for $T_c \leq \tau$ ($T_c = 2^6$). The small fluctuation of $D(\tau)$ around the saturation level may be induced from the discontinuous change of α at k_c. It is noteworthy that $D(\tau)$ does not discontinuously change from D_S to D_L as a step function, but shows a gradual increase as $\tau \to T_c$. Then, even if the time series has a characteristic frequency (f_c) in frequency domain, the $\log\tau$ versus $\log\langle L(\tau)\rangle$ plots have no sharp bent, representing no τ_c.

We also demonstrate in fig. 11 $D(\tau)$ of the time series with a power law index ($\alpha = 2$) in order to confirm the good fit of the straight line to the $\log\tau$ versus $\log\langle L(\tau)\rangle$ plots. $D(\tau)$ exactly agrees with $D = 3/2$ for every τ, except for small τ. The difference between $D(\tau)$ and $D = 3/2$ for small τ comes from truncating the power spectrum at

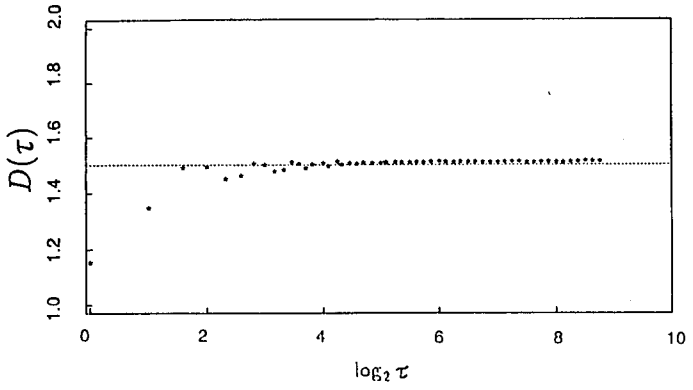

Fig. 11. $D(\tau)$ of the time series with $\alpha = 2$ and $N = 2^{19}$. The phase distribution is random. The dotted horizontal line indicates $D = 3/2$.

the frequency domain higher than $k = N/2$. In short, since the time series constructed by the procedures used in this study has no component within the frequency range higher than $k = N/2$, the self-affinity does not hold within $N/2 < k$. Even if we use a simulated time series with a large N, this effect inevitably occurs as far as N is finite.

5. Summary

For the irregularity of the time series, the randomness of the phase distribution strongly affects the behavior in the time domain. In short, the phase distribution leads to a drastic change in the smoothness of the curve as illustrated in figs. 1a–1e. It was pointed out that we cannot discern between the irregular and smooth functions only by using the power spectrum analysis. For example, even if the power spectrum density of the time series shows a power law form with a power law index of 5/3, which is the same value as that of the classical Kolmogoroff turbulence, it is possible that the time series shows a very smooth behavior in the time domain. Whenever we measure the irregularity of the time series, we should take into account the information about the phase. We also investigated the relationship between the randomness of the phases and the fractal dimension by using simulated data. The value of the fractal dimension changes depending on the probability distribution of the phase of the time series.

When a time series has a power law spectrum within $1 < \alpha < 3$ and a random phase distribution, the time series corresponds to the BLF curve; when $P(k) \propto k^{-\alpha}$, $\theta_k \sim U([0, 360])$, and $\langle \theta_k \theta_{k'} \rangle = \delta_{kk'}$, $X(j)$ is identical with the BLF curve. In this case, the relation between α and D is defined by $\alpha = 5 - 2D$ for the definition domain $1 < \alpha < 3$. All time series with a power law index within $0 \leq \alpha < 1$ possess $D = 2$ and this degeneration can be resolved by calculating D_Σ, which is the fractal dimension of the integrated time series, because D_Σ maps α one-to-one. On the other hand, although any time series within $3 < \alpha < 5$ corresponds to $D = 1$, α can also be estimated through D_∇, which is the fractal dimension of the differenced time series.

Finally, for the time series with a characteristic frequency where the power law index abruptly changes, the relationship between the power law index and the fractal dimension was also examined by using numerical experiments. In this case, we extended the definition of the fractal dimension from D to $D(\tau)$. The fractal dimension, $D(\tau)$, is defined as a function of τ, representing the irregularity of the fluctuations with a time scale of τ.

Acknowledgements

I am grateful to Professor S. Kokubun, who has kept encouraging me through the progress of this study. This work was supported by the Grant-in-Aid for Encouragement of Young Scientists Project 63790198, from Ministry of Education, Science and Culture, Japan.

References

[1] B. Mandelbrot, Fractals: Form, Chance and Dimension (Freeman, San Francisco, 1977).
[2] K.J. Falconer, The Geometry of Fractal Sets (Cambridge Univ. Press, Cambridge, 1985).

[3] M.V. Berry, Diffractals, J. Phys. A 12 (1979) 781.
[4] L.F. Burlaga and L.W. Klein, Fractal structure of the interplanetary magnetic field, J. Geophys. Res. 91 (1986) 347.
[5] T. Higuchi, Approach to an irregular time series on the basis of the fractal theory, Physica D 31 (1988) 277.
[6] D.A. Roberts and M.L. Goldstein, Spectral signatures of jumps and turbulence in interplanetary speed and magnetic field data, J. Geophys. Res. 92 (1987) 10105.
[7] S.R. Brown, A note on the description of surface roughness using fractal dimension, Geophys. Res. Lett. 14 (1987) 1095.
[8] C.G. Fox, Empirically derived relationships between fractal dimension and power law form frequency spectra, Pure Appl. Geophys. 131 (1989) 211.
[9] C.E. Shanon, Bell Syst. Tech. J. 27 (1948) 379.
[10] H. Akaike, Prediction and Entropy, A Celebration of Statistics (Springer, Berlin, 1985) pp. 1–24.
[11] J. Feder, Fractals (Plenum, New York, 1988).